

# Constraining ultralight dark matter using the Fermi-LAT Pulsar Timing Array

Zi-Qing Xia,<sup>1</sup> Tian-Peng Tang,<sup>1,2</sup> Xiaoyuan Huang\*,<sup>1,2</sup> Qiang Yuan†,<sup>1,2</sup> and Yi-Zhong Fan‡<sup>1,2</sup>

<sup>1</sup>Key Laboratory of DM and Space Astronomy, Purple Mountain Observatory,  
Chinese Academy of Sciences, Nanjing 210033, China

<sup>2</sup>School of Astronomy and Space Science, University of Science and Technology of China, Hefei, Anhui 230026, China  
(Dated: March 31, 2023)

Ultralight dark matter (ULDM) is proposed as a theoretical candidate of dark matter particles with masses of approximately  $10^{-22}$  eV. The interactions between ULDM particles and standard model particles would cause variations in pulse arrival times of the pulsars, which makes the pulsar timing array (PTA) can be used to indirectly detect ULDM. In this work, we use the gamma-ray PTA composed of 29 millisecond pulsars observed by the Fermi Large Area Telescope (Fermi-LAT) to test four ultralight dark matter effects, including gravitational effects for generalized ULDM with different Spin-0/1, the fifth-force coupling effect of Dark Photon and the modified gravitational effect of the Spin-2 ULDM. The gamma-ray pulsar timing is not affected by the ionized interstellar medium and suffers relatively simple noises, unlike that of the radio band. No significant signals of ULDM are found based on the Fermi-LAT PTA for all four kinds of ULDM models. Constraints on ULDM parameters are set with the 95% confidence level, which provides a complementary check of the non-detection of ULDM for radio PTAs and direct detection experiments.

PACS numbers:

Keywords:

## I. INTRODUCTION

Dark matter (DM) is believed to make up almost a quarter of the total energy of the current Universe, which is more than five times of ordinary visible matter [1]. Theoretical physicists have proposed various hypothetical particles as dark matter candidates, such as weakly interacting massive particles (WIMPs) [2], axions [3], sterile neutrinos [4] and Dark Photons [5]. The masses of these proposed dark matter particles span a board range from below  $10^{-22}$  eV to above TeV.

Here, we focus on the ultralight dark matter (ULDM) with the mass of  $\sim 10^{-22}$  eV, whose de Broglie wavelength is up to the subgalactic scale ( $\sim 1$  kpc). Compared with other dark matter candidates, ultralight dark matter particles have the advantage in forecasting small-scale structures consistent with observations [6–10]. ULDM models can be roughly classified by the spin of particle: (1) the Spin-0 (scalar or pseudo-scalar) ULDM case, like ultralight axion-like scalar field dark matter [11–16]; (2) the Spin-1 (vector) ULDM case, specially ultralight Dark Photon (DP) [16–21]; (3) the Spin-2 (tensor) ULDM case [22]. Due to the macroscopic de Broglie wavelength, the gravitational effect of generalized ULDM and the coupling effect (usually dubbed the fifth force) of Dark Photon would cause the oscillation of the Earth and pulsars, which would result in the monochromatic periodical variation in the pulse arrival time and provide an interesting method to probe ULDM. Though another multi-field ULDM scenario has been also discussed for a wide-band spectrum in Ref. [23], here we mainly focus on the monochromatic signal induced by ULDM in the nanohertz range.

The Pulsar Timing Array (PTA) experiments have been continuously monitoring a series of highly stable millisecond pulsars for more than a decade, and accurately recording the arrival times of their periodic electromagnetic pulses. Gravitational perturbations could induce variations in the time that pulses take from a millisecond pulsar to the Earth. Therefore, PTA is designed to be an excellent detector for nanohertz-frequency gravitational perturbations from the Gravitational Wave Background (GWB) and the single gravitational wave event, and also for the oscillations induced by ULDM [18, 24–30]. The traditional PTA projects are generally at the radio wavelength: the Parkes Pulsar Timing Array (PPTA) in Australia [31, 32], the European Pulsar Timing Array (EPTA) combining five 100-m class radio-telescopes [33, 34], the North American Nanohertz Observatory for Gravitational Waves (NANOGrav) composed of the Arecibo Telescope and the Green Bank telescope [35, 36] and that for the 500-m aperture spherical radio telescope (FAST) [37, 38]. Recently, a gamma-ray PTA recently have been constructed from the Fermi Large Area Telescope (LAT) data for searching the GWB from merging supermassive black hole (SMBH) binaries [39], which can provide an independent and complementary check for radio PTAs. Also, the gamma-ray PTA has the advantage that it would not involve the uncertainty from the effect of the ionized interstellar medium (IISM) on the propagating path of photons which can induce additional noises in radio PTAs. In this work, the public timing data of the Fermi-LAT PTA<sup>1</sup> is adopted to search for the monochromatic signals produced by the coherent oscillation effect of ULDM particles with the different Spin-0/1/2, including the gravitational effects for ULDM with the Spin-0/1, the coupling (fifth-force) effect of Dark Photon and the modified gravitational effect for

\*Corresponding Author: xyhuang@pmo.ac.cn

†Corresponding Author: yuanq@pmo.ac.cn

‡Corresponding Author: yzf@pmo.ac.cn

<sup>1</sup> <https://zenodo.org/record/6374291#.YzVcbC-KFpR>

the Spin-2 ULDM.

## II. ULTRALIGHT DARK MATTER MODEL

### A. Spin-0: Gravitational Signal

With a macroscopic de Broglie wavelength of galactic scales, the Spin-0 ULDM particles around the Earth-pulsars system would produce the periodic oscillation in gravitational potentials, which could cause sinusoidal variations in the times of arrival (ToA) of pulse. This oscillating effect is similar to the steady monochromatic gravitational wave from a distant source. The Spin-0 ULDM could induce a time-dependent gravitational potential with the frequency ( $f$ ) twice the mass of ULDM particle ( $m$ ) [26]:

$$f = \frac{2m}{2\pi} = 4.8 \times 10^{-9} \text{Hz} \left( \frac{m}{10^{-23} \text{eV}} \right), \quad (1)$$

The corresponding timing residuals of ToAs can be written as [27]:

$$\begin{aligned} s(t) &= \frac{\Psi_e}{2\pi f} \sin(2\pi f t + 2\theta_e) - \frac{\Psi_p}{2\pi f} \sin \left[ 2\pi f \left( t - \frac{d_p}{c} \right) + 2\theta'_p \right] \\ &= \frac{\Psi_e}{2\pi f} \sin(2\pi f t + 2\theta_e) - \frac{\Psi_p}{2\pi f} \sin[2\pi f t + 2\theta_p], \end{aligned} \quad (2)$$

where  $d_p$  is the distance from pulsars in the Fermi-LAT PTA to the Earth,  $\Psi_e$  and  $\Psi_p$  are the amplitude of the oscillating part of the gravitational potential for the Earth and pulsar terms, separately.  $\theta_e$  and  $\theta'_p$  each represent the scalar-field oscillation phases for the Earth and pulsar terms. To simplify the formula, we take the phase of pulsar term as  $\theta_p$  which absorbs the time difference ( $d_p/c$ ) between a pulsar and the Earth.

The amplitude is related to the density of dark matter  $\rho_{\text{DM}}$ ,

$$\Psi = \frac{G\rho_{\text{DM}}}{\pi f^2} \approx 6.1 \times 10^{-18} \left( \frac{m}{10^{-22} \text{eV}} \right)^{-2} \left( \frac{\rho_{\text{DM}}}{\rho_0} \right), \quad (3)$$

where  $\rho_0 = 0.4 \text{ GeV cm}^{-3}$  is the measured local dark matter density near the Earth [40, 41]. Since the pulsar distance  $d_p$  to the Earth are relatively small (for 27 of 29 pulsars below 3 kpc), the dark matter density around pulsars can be approximately considered to be the local density near the Earth. Hence the amplitude for the Earth term and pulsar terms are set to be the same (as implicitly done in Ref [27]), uniformly labeled as  $\Psi$ . Under this assumption and the Eq. (1), the timing residuals of ToAs can be written into

$$s(t) = \frac{\Psi}{m} \sin(\theta_e - \theta_p) \cos(2mt + \theta_e + \theta_p). \quad (4)$$

The prior distributions of  $\theta_p$  and  $\theta_e$  are set to be uniform between 0 to  $2\pi$  as listed in Tab. I. The whole derivation of Eq. (4) is presented in Refs. [26, 27].

### B. Spin-1: Gravitational Signal

Same with the Spin-0 model, the oscillation of gravitational potential induced by the Spin-1 ULDM could also result in

periodic timing signals in observations of PTAs, with the frequency twice the ULDM mass as in the Eq. (1). However, the Spin-1 gravitational timing signals is related to the oscillation direction of the vector field, which is a distinctive feature different from the Spin-0 case. This signal has been derived in detail in the Refs [18, 30], which can be generally divided into two parts. One is  $s_\Psi(t)$  for the gravitational potentials:

$$s_\Psi(t) = \frac{\Psi_{\text{osc}}}{m} \sin(\theta_e - \theta_p) \cos(2mt + \theta_e + \theta_p), \quad (5)$$

where  $m$  is the mass of the Spin-1 ULDM particle,  $\Psi_{\text{osc}}$  represents the corresponding amplitude of potential,  $\theta_e$  and  $\theta_p$  are oscillation phases for the Earth and pulsar terms, separately. The other is  $s_h(t)$  for the traceless spatial metric perturbations exhibiting the anisotropy for additional degrees of freedom in the vector field and does not exist in the Spin-0 case:

$$s_h(t) = -\frac{1}{4} (1 + 3 \cos 2\theta) \frac{h_{\text{osc}}}{m} \sin(\theta_e - \theta_p) \cos(2mt + \theta_e + \theta_p), \quad (6)$$

where  $h_{\text{osc}}$  is the amplitude of perturbations,  $\theta$  is the angle between the line of sight to a pulsar and the oscillation direction of the vector ULDM ( $\theta_{\text{osc}}, \phi_{\text{osc}}$ ). The amplitudes for these two oscillation parts also depend on local DM density  $\rho_{\text{DM}}$  and can be given as, respectively:

$$\Psi_{\text{osc}} = -\frac{\pi G \rho_{\text{DM}}}{3m^2} \approx -2.2 \times 10^{-18} \left( \frac{m}{10^{-22} \text{eV}} \right)^{-2} \left( \frac{\rho_{\text{DM}}}{\rho_0} \right), \quad (7)$$

$$h_{\text{osc}} = \frac{8\pi G \rho_{\text{DM}}}{3m^2} \approx 1.7 \times 10^{-17} \left( \frac{m}{10^{-22} \text{eV}} \right)^{-2} \left( \frac{\rho_{\text{DM}}}{\rho_0} \right), \quad (8)$$

where the measured local DM density is taken as  $\rho_0 = 0.4 \text{ GeV cm}^{-3}$  (same as above). Combining these two parts of oscillation, we get the total Spin-1 gravitational timing signal written as

$$\begin{aligned} s(t) &= s_\Psi(t) + s_h(t) \\ &= -\frac{3}{8} (1 + 2 \cos 2\theta) \frac{h_{\text{osc}}}{m} \sin(\theta_e - \theta_p) \cos(2mt + \theta_e + \theta_p), \end{aligned} \quad (9)$$

which is angle-dependent, unlike the Spin-0 model. When the vector field oscillates along with the line-of-sight direction, the maximal amplitude was found as three times larger than that of the Spin-0 case [18]. With the PPTA second data release (DR2) dataset, the Ref. [30] has not found a preferred oscillation direction of the Spin-1 ULDM ( $\theta_{\text{osc}}, \phi_{\text{osc}}$ ) which are also set as free parameters in our work.

### C. Spin-1: Fifth-Force Signal

As a special case of the Spin-1 ULDM candidates, the Dark Photon is the hypothetical gauge boson of a  $U(1)$  interaction proposed by the string theory [42–44]. The mass of Dark Photon could be generated by the Higgs mechanism or the Stueckelberg mechanism, and it is naturally light. If

TABLE I: The parameters of signal and noise models for the analysis.

Model	Parameter	Prior	Description
Spin-0: Gravitational Signal	$\theta_p$	$U[0, 2\pi]$	Phase for the pulsar term, one per pulsar
	$\theta_e$	$U[0, 2\pi]$	Phase for the Earth term, one per PTA
	$\Psi$	$\log\text{-}U[10^{-20}, 10^{-12}]$	Oscillation amplitude for the Spin-0 ULDM field, one per PTA
	$m$	$\log\text{-}U[10^{-24}, 10^{-21}]$	Mass for the Spin-0 ULDM, one per PTA
Spin-1: Gravitational Signal	$\theta_p$	$U[0, 2\pi]$	Phase for the pulsar term, one per pulsar
	$\theta_e$	$U[0, 2\pi]$	Phase for the Earth term, one per PTA
	$\theta_{\text{osc}}$	$U[0, \pi]$	Polar angle of the Spin-1 ULDM oscillation direction, one per PTA
	$\phi_{\text{osc}}$	$U[0, 2\pi]$	Azimuth angle of the Spin-1 ULDM oscillation direction, one per PTA
	$h_{\text{osc}}$	$\log\text{-}U[10^{-19}, 10^{-9}]$	Oscillation amplitude for the Spin-1 ULDM field, one per PTA
	$m$	$\log\text{-}U[10^{-24}, 10^{-21}]$	Mass for the Spin-0 ULDM, one per PTA
Spin-1: Fifth-Force Signal	$\theta_p$	$U[0, 2\pi]$	Phase for the pulsar term, one per pulsar
	$\theta_e$	$U[0, 2\pi]$	Phase for the Earth term, three per PTA
	$(\tilde{A}_0)^2$	$f(x) = e^{-x}$	Normalized gauge potential of the Dark Photon field, three per PTA
	$\epsilon$	$\log\text{-}U[10^{-28}, 10^{-16}]$	Coupling strength for the Dark Photon field, one per PTA
	$m$	$\log\text{-}U[10^{-24}, 10^{-21}]$	Mass for the Dark Photon, one per PTA
Spin-2: Modified Gravitational Signal	$\theta_p$	$U[0, 2\pi]$	Phase for the pulsar term, one per pulsar
	$\theta_e$	$U[0, 2\pi]$	Phase for the Earth term, one per PTA
	$\alpha$	$\log\text{-}U[10^{-12}, 10^{-1}]$	Coupling strength for the Spin-2 ULDM field, one per PTA
	$m$	$\log\text{-}U[10^{-24}, 10^{-21}]$	Mass for the Spin-2 ULDM, one per PTA
White Noise (WN)	EFAC	$U[0, 1.5]$	Re-scaling factor, one per pulsar
	EQUAD	$\log\text{-}U[10^{-9}, 10^{-5}]$	Extra white noise, one per pulsar
Red Noise (RN)	$A$	$\log\text{-}U[10^{-18}, 10^{-9}]$	Amplitude for red noise, one per pulsar
	$\gamma$	$U[0, 7]$	Index for red noise, one per pulsar
BayesEphem Noise (BEph)	$z_{\text{drift}}$	$U[-10^{-9}, 10^{-9}]$	Drift-rate of Earth's orbit about ecliptic z-axis, one per PTA
	$\Delta M_{\text{Jupiter}}$	$N(0, 1.5 \times 10^{-11})$	Perturbation of Jupiter's mass, one per PTA
	$\Delta M_{\text{Saturn}}$	$N(0, 8.2 \times 10^{-12})$	Perturbation of Saturn's mass, one per PTA
	$\Delta M_{\text{Uranus}}$	$N(0, 5.7 \times 10^{-11})$	Perturbation of Uranus' mass, one per PTA
	$\Delta M_{\text{Neptune}}$	$N(0, 7.9 \times 10^{-11})$	Perturbation of Neptune's mass, one per PTA
	$\text{PCA}_i$	$U[-0.05, 0.05]$	Principal components of Jupiter's orbit, six per PTA

the  $U(1)$  symmetry is for the baryon number (the  $U(1)_B$  interaction) or for the baryon-minus-lepton number (the  $U(1)_{B-L}$  interaction), there would be the “fifth-force” interaction with the ordinary matter, which could be used to probe the Dark Photon. Ref [21] has compared the pure gravitational effect for the vector ULDM with the “fifth-force” effect and find the “fifth force” could produce larger timing residuals when  $\epsilon \times m_A \text{eV} > 10^{-48.35}$  for the  $U(1)_B$  scenario and  $10^{-48.24}$  for the  $U(1)_{B-L}$  scenario. Here we consider the effect from the “fifth force” for the Dark Photon case, instead of the previously introduced gravitational effect.

The frequency of the oscillating signal in timing residuals caused by the “fifth force” is given by m:

$$f = \frac{m}{2\pi} = 2.4 \times 10^{-9} \text{Hz} \left( \frac{m}{10^{-23} \text{eV}} \right). \quad (10)$$

And the “fifth force” induced by Dark Photon with the mass of  $m$  can give an acceleration on the test mass  $m_t$  located at  $\mathbf{x}$  [21, 45]:

$$\mathbf{a}(t, \mathbf{x}) \simeq \epsilon e \frac{q}{m_t} m \mathbf{A}_0 \cos(mt - \mathbf{k} \cdot \mathbf{x} + \theta(\mathbf{x})), \quad (11)$$

where  $\epsilon$  is the coupling strength of the new  $U(1)$  gauge interaction (normalized to the electromagnetic coupling constant  $e$ ),  $q$  counts the number of the baryon ( $B$ ) or the neutron (baryon-minus-lepton,  $B-L$ ) and  $\mathbf{k}$  represents the characteristic momentum.  $\mathbf{A}_0$  and  $\theta$  are on behalf of the gauge potential

and phase of the Dark Photon field, respectively. The amplitude of  $\mathbf{A}_0$  depends on the dark matter density which we set to the observed local dark matter density  $\rho_0 = 0.4 \text{ GeV cm}^{-3}$ . The averaged value of the amplitude can be given by  $|\mathbf{A}_0|^2 = 2\rho_0/m^2$ . And we assume there is a common amplitude  $\mathbf{A}_0$  of Dark Photon field around the Earth and pulsars. The displacement caused by the acceleration can be approximately given as

$$\Delta \mathbf{x}(t, \mathbf{x}) = -\frac{\epsilon e q}{m m_A} \mathbf{A}_0 \cos(mt - \mathbf{k} \cdot \mathbf{x} + \theta(\mathbf{x})). \quad (12)$$

Hence, the total periodic timing residuals caused by the “fifth-force” effect is a combination of the Earth (labeled as  $e$ ) term and pulsar (labeled as  $p$ ) term, which has been derived in our previous work [21]:

$$s(t)^{(B)} = \frac{\epsilon e}{m} \mathbf{A}_0 \left[ \frac{q_e^{(B)}}{m_e} \cos(mt + \theta_e) - \frac{q_p^{(B)}}{m_p} \cos(mt + \theta_p) \right] \cdot \mathbf{n}, \quad (13)$$

$$s(t)^{(B-L)} = \frac{\epsilon e}{m} \mathbf{A}_0 \left[ \frac{q_e^{(B-L)}}{m_e} \cos(mt + \theta_e) - \frac{q_p^{(B-L)}}{m_p} \cos(mt + \theta_p) \right] \cdot \mathbf{n}, \quad (14)$$

where  $\mathbf{n}$  is the normalized position vector pointing from the Earth to the pulsar,  $q_{e,p}^{(B)}$ ,  $q_{e,p}^{(B-L)}$ ,  $m_{e,p}$  each represent the  $B$  number, the  $B-L$  number, the mass of the Earth and the pulsar. For the  $U(1)_B$  interaction,  $q^{(B)}/m$  can be roughly taken as 1/GeV for both the Earth and the pulsar. While for  $U(1)_{B-L}$ ,  $q^{(B-L)}/m$  is approximately 0.5/GeV for the Earth and 1/GeV for the pulsar. The detailed derivations of Eq. (13) and Eq. (14) can be found in Ref. [21].

#### D. Spin-2: Modified Gravitational Signal

The massive Spin-2 field is proposed as a modification of gravity and behaves as a potential dark matter candidate [46, 47]. A direct coupling with the energy-momentum tensor of standard matter is naturally involved by the tensorial structure and action of the Spin-2 ULDM, which can be parametrized by the dimensionless strength constant  $\alpha$ . The oscillating frequency  $f$  for the Spin-2 case is given by  $m$ , which is the same as the Eq. (10) for the Dark Photon. Based on the bimetric gravity, Ref. [22] detailedly describe the effect of any universally-coupled Spin-2 ULDM on the PTA. For the Spin-2 case, we approximately take  $\rho_0 = 0.4 \text{ GeV cm}^{-3}$  as dark matter density  $\rho_{DM}$  for both the pulsar term and the Earth term. Conducted from the Eq.(A.10) in Ref. [22], we obtained the time residual as:

$$s(t) = \frac{\alpha \sqrt{2\rho_0}}{\sqrt{15}m^2 M_P} \cos(mt + \frac{\theta_e + \theta_p}{2}), \quad (15)$$

where  $M_P$  is the reduced Planck mass, and  $\theta_p$  includes the time difference ( $d_p/c$ ) from a pulsar to the Earth. Prior distributions of Spin-2 model parameters are summarized in Tab. I.

### III. THE FERMI-LAT PTA

#### A. Data

The Fermi-LAT collaboration use 12.5 yr of Fermi-LAT data from 2008 Aug 04 to 2021 Jan 28 to form the first gamma-ray PTA, or called the Fermi-LAT PTA. It is composed of the 35 brightest and most stable gamma-ray millisecond pulsars (MSPs). However, only 29 of 35 MSPs in the Fermi-LAT PTA can be efficiently estimated ToAs of pulses, and are suitable for the ToA-based method which is widely used in radio PTAs. In this work, we also adopt the ToA-based method and use the ToAs data recorded in the .tim files for these 29 MSPs which is the Full 29 set in Ref. [39]. Tab. III lists pulsar name, the cadence chosen, distance  $d_p$ , median ToA uncertainty  $\sigma_{\text{ToA}}$  and the weighted root-mean-square of timing residuals  $rms$  for each pulsar.

The Fermi-LAT PTA has calculated ToAs by a cadence of 2, 1.5, and 1 yr<sup>-1</sup> and obtained a total of 25, 19, and 12 ToAs for each pulsar. The ToAs with a higher cadence can provide more high-frequency information and larger data volume. Hence, in a general way, the 2 yr<sup>-1</sup> cadence is a relatively optimal choice. However, PSR J0533+6759, PSR J0740+6620,

TABLE II: The basic information for 29 millisecond pulsars in the Fermi-LAT PTA: Cadence is the cadence adopted in the analysis;  $d_p$  is the best estimate of the pulsar distance using the YMW16 DM-based distance taken from the ATNF Pulsar Catalogue<sup>a</sup> [48];  $\sigma_{\text{ToA}}$  is the median ToA uncertainty for the Fermi-LAT PTA data; rms is the weighted root-mean-square of timing residuals; Noise Model shows the favored additional noise model for each pulsar taken from the Ref. [39]. The distance of PSR J2034+3632 is missing and set to be 1 kpc as default.

Pulsar Name (PSR)	Cadence (ToA/yr)	$d_p$ (kpc)	$\sigma_{\text{ToA}}$ ( $\mu\text{s}$ )	rms ( $\mu\text{s}$ )	Noise Model (favored)
J0030+0451	2	0.32	4.13	4.32	None <sup>b</sup>
J0034-0534	2	1.35	13.41	10.11	None
J0101-6422	2	1.00	14.16	16.85	None
J0102+4839	2	2.31	16.14	19.18	None
J0340+4130	2	1.60	18.26	23.03	None
J0533+6759	1.5	2.40	16.80	13.30	None
J0613-0200	2	0.78	19.41	14.46	None
J0614-3329	2	0.63	2.53	2.71	None
J0740+6620	1.5	1.15	10.53	2.34	None
J1124-3653	2	0.99	10.33	3.13	None
J1231-1411	2	0.42	2.43	2.51	None
J1514-4946	2	0.91	12.48	14.22	None
J1536-4948	2	0.98	7.02	7.01	None
J1614-2230	2	0.70	5.80	10.35	None
J1625-0021	1.5	0.95	18.52	15.27	None
J1630+3734	2	1.19	5.82	5.64	None
J1810+1744	2	2.36	10.26	12.44	None
J1816+4510	2	4.36	19.72	25.01	None
J1858-2216	2	0.92	13.10	19.05	None
J1902-5105	2	1.65	7.84	7.62	None
J1939+2134	1.5	3.50	7.20	11.45	None
J1959+2048	2	1.40	4.78	9.35	WN
J2017+0603	2	1.40	14.38	19.94	None
J2034+3632	1.5	—	17.59	18.73	None
J2043+1711	2	1.39	8.04	9.29	None
J2214+3000	2	0.60	20.09	23.94	None
J2241-5236	2	1.04	5.30	6.57	WN
J2256-1024	1.5	2.08	4.13	5.23	None
J2302+4442	2	0.86	11.38	8.20	None

<sup>a</sup><https://www.atnf.csiro.au/research/pulsar/psrcat/>

<sup>b</sup>“None” means that there is no additional noise found and the white noise equals to measured ToA uncertainties.

PSR J1625-0021, PSR J1939+2134, PSR J2034+3632, and PSR J2256-1024 are relatively faint in all 29 MSPs and exhibit more systematic error with the 2 yr<sup>-1</sup> cadence than that for the longer integration [39]. For these 6 MSPs, the reliable ToAs produced with the 1.5 yr<sup>-1</sup> cadence are adopted in the following analysis, which is the same as the preferred cadence in Ref. [39].

#### B. Timing Model

The ToAs of a pulsar can be reconstructed from three parts:

$$\text{ToA} \sim t_{\text{TM}} + \Delta t_{\text{Noise}} + s(t). \quad (16)$$



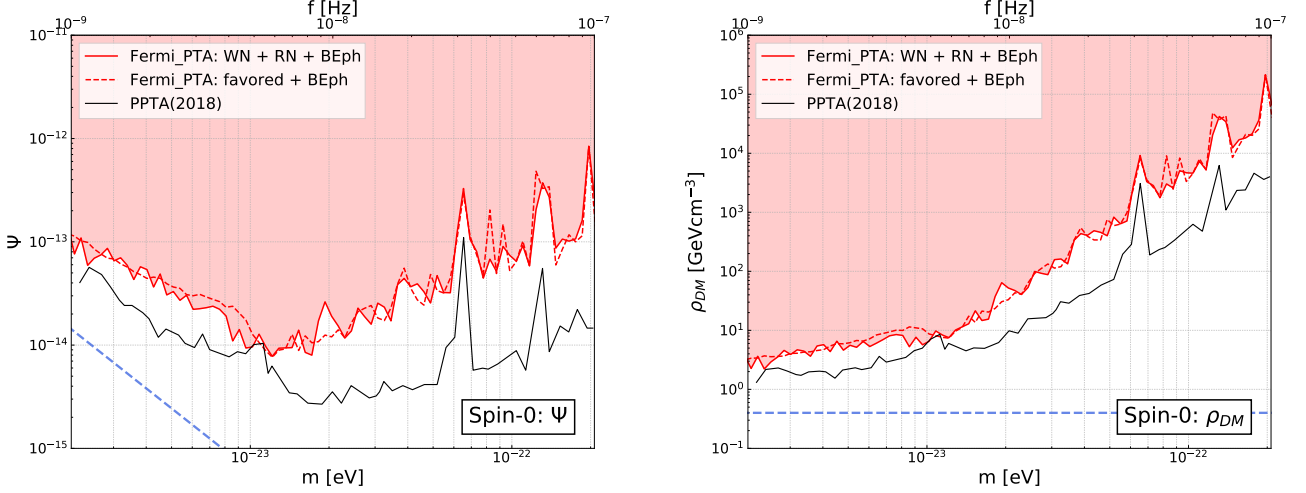


FIG. 1: Constraints on the gravitational effect for the Spin-0 case: The left panel shows the 95% confidence level upper limits of oscillation amplitude  $\Psi$ . The right panel shows limits on the local dark matter density  $\rho_{DM}$ . For both panels, red solid lines are upper limits with all noise (WN + RN + BEph) components, while red dashed lines are for the case only including the favored noise model (as listed in Tab. III) and the BayesEphem uncertainty (favored + BEph). The blue dashed lines are on behalf of the case that the local DM density  $\rho_{DM}$  equals to the current measurement  $\rho_0 = 0.4 \text{ GeV cm}^{-3}$ . The black lines represent upper limits obtained by PPTA in 2018 [27].

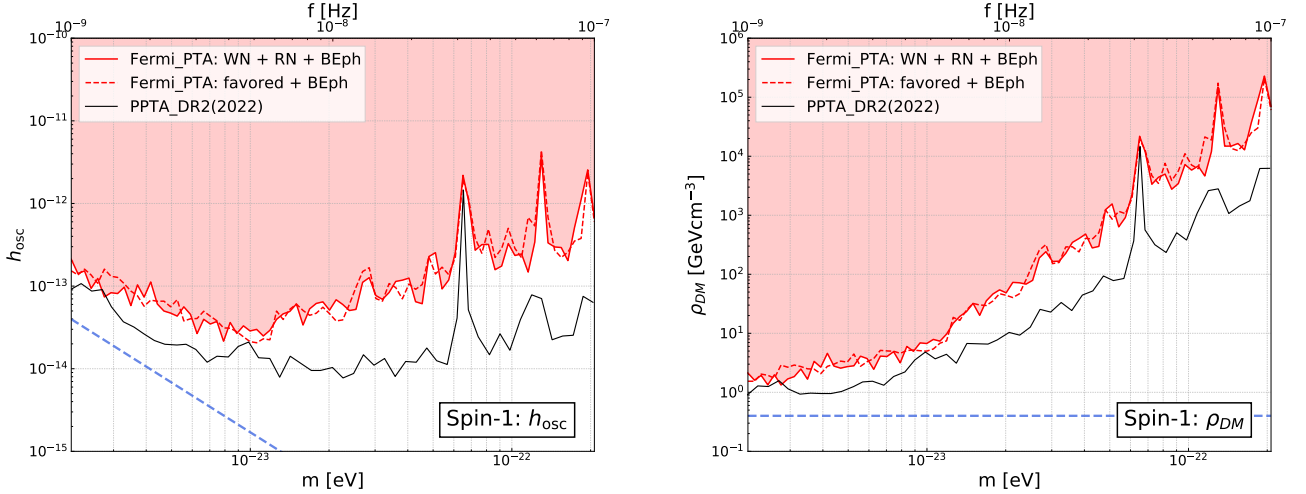


FIG. 2: Constraints on the gravitational effect for the Spin-1 case: The left panel shows the 95% confidence level upper limits of oscillation amplitude  $h_{osc}$ . The right panel shows limits on the local dark matter density  $\rho_{DM}$ . For both panels, red solid lines are upper limits with all noise (WN + RN + BEph) components, while red dashed lines are for the case only including the favored noise model (as listed in Tab. III) and the BayesEphem uncertainty (favored + BEph). The blue dashed lines represent the case of the local DM density  $\rho_{DM} = 0.4 \text{ GeV cm}^{-3}$ . The previous upper limits based on PPTA DR2 are given as the black lines [30].

The first term  $t_{TM}$  is on behalf of the timing model accounting for the pulsar ephemeris. In this work, we use the optimized ephemerides model given by Ref. [39]<sup>2</sup> and marginalize over model uncertainties. The second term  $\Delta t_{Noise}$  is the timing

residual contributed by noises. The third term  $s(t)$  is the timing residual induced by the signal for each ULDM effect described in Sec. II. The noise parameters, signal parameters and their prior distributions are indicated in Tab. I.

<sup>2</sup> The corresponding .par files can be found in <https://zenodo.org/record/6374291#.YzVcbC-KFpR>.

The noises of PTA can be classified into three categories: the white (time-uncorrelated) noise (WN), the red (time-correlated) noise (RN), and the BayesEphem noise (BEph),

respectively:

$$\Delta t_{\text{Noise}} = \Delta t_{\text{WN}} + \Delta t_{\text{RN}} + \Delta t_{\text{BEph}}. \quad (17)$$

The white noise of the Fermi-LAT PTA is the ToA bias, which could be larger than measured ToA uncertainties. For each pulsar, the white noise can be added by modifying the measurement uncertainty,  $\sigma$ , of ToA:

$$\sigma_s^2 = (\text{EFAC} \times \sigma)^2 + \text{EQUAD}^2, \quad (18)$$

where EFAC is a re-scaling factor and EQUAD is an extra uncertainty. Ref. [39] has made a single-pulsar noise analysis for all 29 pulsars and found that only PSR J1959+2048 and PSR J2241-5236 show a preference for a model with the excess white noise. The red noise of the Fermi-LAT PTA is mainly contributed by the intrinsic pulsar Spin-down power (called the spin noise), which can be adequately modeled with a power-law spectrum:

$$P(f) = \frac{A^2}{12\pi^2} \left( \frac{f}{\text{yr}^{-1}} \right)^{-\gamma} \text{yr}^3, \quad (19)$$

where  $A$  and  $\gamma$  represent the amplitude and spectral index of the power-law power spectral density, respectively. For the radio PTA, there are other components of the red noise: dispersion measure (DM) variations are induced by the variable IISM in the line of sight. But for the Fermi-LAT PTA, the gamma-ray timing is immune to the IISM effect. According to the result of Ref. [39], no evidence for red noise is found in each of all 29 pulsars. The BayesEphem noise accounts for the systematic uncertainty of the DE421 Solar System ephemeris (SSE), which is adopted in this work, with a Bayesian modeling technique [49]. There are 11 parameters for the BayesEphem noise: the drift-rate parameter for the semi-major axis of Earth-Moon barycenter orbit, 4 perturbation parameters for the masses of outer planets, and 6 parameters for principal components parameters of Jupiter's orbit. For the sake of conservation, we consider white and red noises for each pulsar and the BayesEphem noise for the PTA, and marginalize over their parameters in the likelihood analysis to search for the potential ULDM signal.

## IV. ANALYSIS AND RESULT

### A. Data analysis

To search for the signal of ULDM with the Fermi-LAT PTA, we perform the likelihood analysis for two models: the signal model (labeled as  $H_1$ ) given in Eq. (16) and the null model ( $H_0$ ) without timing residual contributed from the ULDM signal ( $s(t)$ ). The PINT software package<sup>3</sup> [51] and enterprise package<sup>4</sup> [52] are used to build the timing model

of ToAs and perform the likelihood analysis. Then we use the PTMCMC package<sup>5</sup> [53] as the stochastic sampling for the posterior probabilities of model parameters to obtain the best-fit parameters. In the case of the  $H_1$  model, we repeat the analysis for each ULDM effect introduced in Sec. II, respectively. In order to compare models with and without signal, we take the likelihood ratio test between the  $H_1$  and  $H_0$  models. The likelihood ratio ( $\lambda_{\text{LR}}$ ) can be given by [54]:

$$\lambda_{\text{LR}} = 2 \ln \frac{\mathcal{L}_{\text{max}}(H_1)}{\mathcal{L}_{\text{max}}(H_0)}, \quad (20)$$

where  $\mathcal{L}_{\text{max}}(H_1)$  and  $\mathcal{L}_{\text{max}}(H_0)$  represent the maximum likelihood values we get for the  $H_1$  and  $H_0$ , respectively. According to Wilks' theorem, the likelihood ratio [54] follows the chi-squared distribution ( $\chi^2$ ) with degrees of freedom equal to the difference in numbers of parameters for the  $H_1$  and  $H_0$ .

Then we further derive constraints on the parameters of ULDM for each effect. For a set of fixed ULDM mass  $m$  in the corresponding frequency  $f$  range ( $10^{-9}$  Hz,  $10^{-7}$  Hz), we sample the posterior probabilities of ULDM parameters with the numerical marginalization for all noise (WN + RN + BEph) parameters mentioned above. When posterior probabilities in the range of  $[0, x_{ul}]$  equal to 95%, we take  $x_{ul}$  as the 95% confidence level upper limit of one ULDM parameter ( $x$ ) for the fixed ULDM mass  $m$ . The upper limit calculation has been made for four kinds of ULDM effects, separately. For completeness, we also calculated upper limits for the case only with favored noise models as listed in Tab. III and the BayesEphem uncertainty, labeled as (favored + BEph).

### B. Result

- Spin-0: Gravitational Signal — Considering the gravitational effect of the Spin-0 ULDM, we get the likelihood ratio  $\lambda_{\text{LR, Spin-0}}$  equals to 3.9 with the best-fit parameters ( $m, \Psi$ ) = ( $1.38 \times 10^{-24}$  eV,  $1.16 \times 10^{-19}$ ). Considering the  $\chi^2$  distribution with 32 degrees of freedom, the corresponding statistical significance is approximate to zero. Hence, the Fermi-LAT PTA shows no evidence for the signal from the Spin-0 ULDM, which is consistent with the result of PPTA [27]. We calculate the 95% confidence level upper limits of oscillation amplitude  $\Psi$  for a set of fixed mass  $m$  corresponding to the frequency from  $10^{-9}$  Hz to  $10^{-7}$  Hz, which are shown in the left panel of Fig. 1. According to the Eq. (3), we then conduct the 95% upper limits of local dark matter density  $\rho_{\text{DM}}$  and exhibit them in the right panel of Fig. 1. The red solid/dashed lines are for the (WN + RN + BEph)/(favored + BEph) noise models. Our constraints on the local dark matter density  $\rho_{\text{DM}}$  is larger than the observed local dark matter density  $\rho_0 = 0.4 \text{ GeV cm}^{-3}$  and higher than upper limits obtained by PPTA in 2018 [27] which is shown as the black lines in Fig. 1.

- Spin-1: Gravitational Signal — As for the gravitational signal of the Spin-1 case, the best-fit parameters we get are

<sup>3</sup> <https://github.com/nanograv/pint>

<sup>4</sup> <https://github.com/nanograv/enterprise>

<sup>5</sup> <https://github.com/jellis18/PTMCMCSampler>

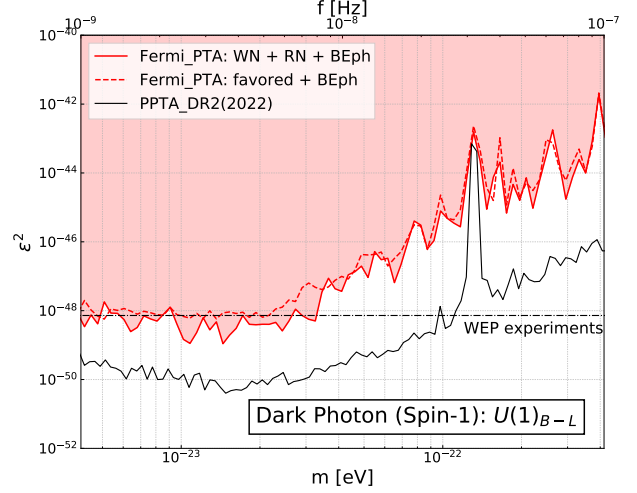
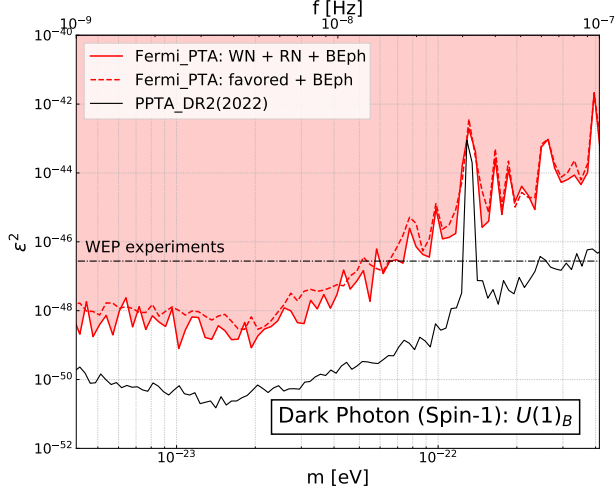


FIG. 3: Constraints on the fifth-force effect of the Dark Photon (Spin-1) model: The left panel shows the 95% confidence level upper limits of the coupling strength  $\epsilon$  for the  $U(1)_B$  scenario, while the right panel is for the  $U(1)_{B-L}$  scenario. The red solid lines are for the (WN + RN + BEph) noise model, while red dashed lines are for the (favored + BEph) noise model. The black lines show limits based on the PPTA DR2 dataset given in Ref. [21]. The horizontal black dash-dot lines are upper limits for the MICROSCOPE WEP experiment [50].

$(m, h_{\text{osc}}) = (1.09 \times 10^{-23} \text{ eV}, 6.11 \times 10^{-16})$ , and the corresponding likelihood ratio is  $\lambda_{\text{LR, Spin-1}} = 3.8$  following the  $\chi^2$  distribution with 34 degrees of freedom. Same as above, we find no significant evidence for the Spin-1 gravitational signal, which is consistent with the result of PPTA DR2 [30]. The Fig. 2 displays the 95% confidence level upper limits with the Fermi-LAT PTA for the oscillation amplitude  $h_{\text{osc}}$  (left panel) and the dark matter density  $\rho_{\text{DM}}$  (right panel) conducted from the Eq. (8). Larger than  $0.4 \text{ GeV cm}^{-3}$  for all the mass range, our limits for the Spin-1 case also cannot set effective constraints on the mass of ULDM particle.

• **Spin-1: Fifth-Force Signal** — In the case of Dark Photon, we consider the two new interaction ( $U(1)_B$  and  $U(1)_{B-L}$ ) scenarios for the Dark Photon. For  $U(1)_B / U(1)_{B-L}$  scenario, best-fit parameters we get are  $(m, \epsilon) = (6.76 \times 10^{-22} \text{ eV}, 9.95 \times 10^{-26}) / (1.36 \times 10^{-22} \text{ eV}, 5.03 \times 10^{-23})$ , respectively. Corresponding likelihood ratios of  $\lambda_{\text{LR, DP}} = 2.1 / 25.2$  are asymptotically the  $\chi^2$  distribution with 37 degrees of freedom and have a statistical significance of  $\sim 0$ . There is no significant signal for both interaction scenarios. The 95% confidence level upper limits of coupling strength  $\epsilon$  for the  $U(1)_B$  and  $U(1)_{B-L}$  scenarios are presented in the left and right panels of Fig. 3, respectively. Our constraints are found weaker than upper limits from the PPTA DR2 [21]. Especially for the  $U(1)_B$  scenario with masses below  $\sim 7 \times 10^{-23} \text{ eV}$ , we set stronger constraints than limits from the MICROSCOPE WEP experiment [50] shown as the horizontal black dash-dot line in Fig. 3.

• **Spin-2: Modified Gravitational Signal** — As for the Spin-2 ULDM model, we obtain the best-fit parameters as  $(m, \alpha) = (1.43 \times 10^{-23} \text{ eV}, 1.45 \times 10^{-6})$  with the likelihood ratio of  $\lambda_{\text{LR, Spin-2}} = 7.3$ . Following the  $\chi^2$  distribution with 32 degrees of freedom, this likelihood ratio corresponds to a significance close to 0. No significant signal is found with the gamma-ray

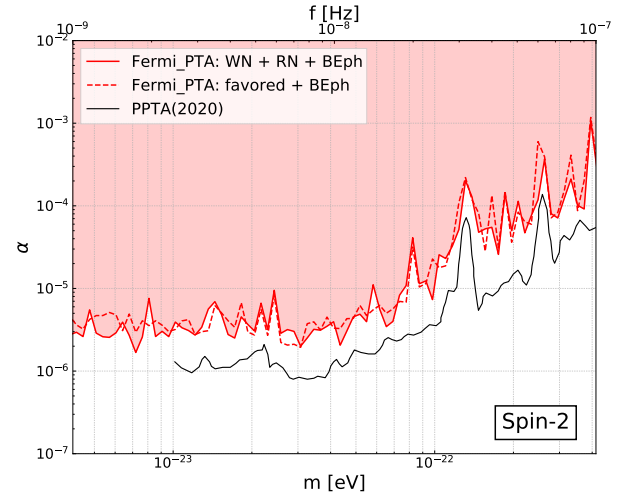


FIG. 4: The 95% confidence level upper limits of the coupling strength  $\alpha$  for the Spin-2 ULDM model. The black line indicates the upper limit set by the PPTA data in Ref. [22].

PTA. Hence, the 95% confidence level upper limits of coupling strength  $\alpha$  are further derived for a set of fixed masses of the Spin-2 ULDM particles as shown in the Fig. 4, which is also weaker than that from PPTA [22].

## V. SUMMARY

ULDM is a theoretical form of dark matter that consists of extremely light particles with masses of  $\sim 10^{-22} \text{ eV}$  beyond the standard model. PTA is a valuable tool for searching

for these ULDM. The idea behind is that the (gravitational or fifth-force) interactions between ULDM particles and standard model particles could cause slight variations in the pulse arrival times, which can be precisely measured by observing the pulsars over long periods of time. If enough pulsars are monitored with the high precision, it may be possible to detect the signature of ULDM in the pulse arrival times.

In this work, we use the gamma-ray PTA which constructed from the Fermi-LAT observation of 29 MSPs to indirectly detect ULDM. Compared with the radio PTAs, the gamma-ray PTA is not affected by the IISM along the line of sight which could induced remarkable red noises for the radio PTAs. Utilizing the traditional ToA-based method, here we search for four ULDM models including the gravitational effects for ULDM particles with the different Spin-0/1, the coupling (fifth-force) effect of Dark Photon and the modified gravitational effect for the Spin-2 ULDM. For all four kinds of ULDM effects, we don't found any significant signal based on the Fermi-LAT PTA dataset, which agree with the non-detection of ULDM signal from radio PTAs and direct detection experiment. Then we further set limits on the parameters of ULDM with the 95% confidence level in the corresponding frequency  $f$  range of ( $10^{-9}$  Hz,  $10^{-7}$  Hz). As for the Spin-0/1 gravitational effects, our constraints are larger than the measured local DM density  $\rho_0 = 0.4 \text{ GeV cm}^{-3}$  and thus hard

to further limit the particle mass of ULDM. In the case of the Spin-1 Dark Photon effect, our constraints for the  $U(1)_B$  scenario with masses below  $\sim 7 \times 10^{-23} \text{ eV}$  is more competitive than that of the MICROSCOPE WEP experiment. For all the four effects, our limits based on the gamma-ray PTA are weaker than those of radio PTAs, due to the relatively smaller amounts of timing data. However our work could be an independent and complementary check for the ULDM detection based on radio PTAs.

In the near future, the Very Large Gamma-ray Space Telescope (VLAST) [55], one of the next generation space-based gamma-ray telescope with a detection area of  $\sim 10^5 \text{ cm}^2$ , will be helpful to establish a stronger gamma-ray PTA to probe the ULDM and even the nanohertz-frequency gravitational waves.

### Acknowledgments

This work is supported by the National Key Research and Development Program of China (No. 2022YFF0503304), the Natural Science Foundation of China (No. 12003069, 11921003), the Chinese Academy of Sciences, and the Entrepreneurship and Innovation Program of Jiangsu Province.

- 
- [1] Planck Collaboration *et al.*, “Planck 2015 results. XIII. Cosmological parameters,” *Astron. Astrophys* **594**, A13 (2016), [arXiv:1502.01589](#).
  - [2] K. Garrett and G. Dūda, “Dark Matter: A Primer,” *Advances in Astronomy* **2011**, 968283 (2011), [arXiv:1006.2483](#).
  - [3] S. Weinberg, “A new light boson?” *Phys. Rev. Lett.* **40**, 223 (1978).
  - [4] A. Boyarsky, M. Drewes, T. Lasserre, S. Mertens, and O. Ruchayskiy, “Sterile neutrino Dark Matter,” *Progress in Particle and Nuclear Physics* **104**, 1 (2019), [arXiv:1807.07938](#).
  - [5] R. Essig *et al.*, “Dark Sectors and New, Light, Weakly-Coupled Particles,” [arXiv e-prints](#), [arXiv:1311.0029](#) (2013), [arXiv:1311.0029](#).
  - [6] W. Hu, R. Barkana, and A. Gruzinov, “Fuzzy Cold Dark Matter: The Wave Properties of Ultralight Particles,” *Phys. Rev. Lett.* **85**, 1158 (2000), [arXiv:astro-ph/0003365](#).
  - [7] J. Zhang, Y.-L. Sming Tsai, J.-L. Kuo, K. Cheung, and M.-C. Chu, “Ultralight Axion Dark Matter and Its Impact on Dark Halo Structure in N-body Simulations,” *Astrophys. J.* **853**, 51 (2018), [arXiv:1611.00892](#).
  - [8] J. S. Bullock and M. Boylan-Kolchin, “Small-Scale Challenges to the  $\Lambda$ CDM Paradigm,” *Annu. Rev. Astron. Astrophys.* **55**, 343 (2017), [arXiv:1707.04256](#).
  - [9] E. Kendall and R. Easther, “The core-cusp problem revisited: ULDM vs. CDM,” *Publ. Astron. Soc. Australia* **37**, e009 (2020), [arXiv:1908.02508](#).
  - [10] J. C. Niemeyer, “Small-scale structure of fuzzy and axion-like dark matter,” *Progress in Particle and Nuclear Physics* **113**, 103787 (2020), [arXiv:1912.07064](#).
  - [11] N. K. Porayko and K. A. Postnov, “Constraints on ultralight scalar dark matter from pulsar timing,” *Phys. Rev. D* **90**, 062008 (2014), [arXiv:1408.4670](#).
  - [12] L. Hui, J. P. Ostriker, S. Tremaine, and E. Witten, “Ultralight scalars as cosmological dark matter,” *Phys. Rev. D* **95**, 043541 (2017), [arXiv:1610.08297](#).
  - [13] D. Blas, D. L. Nacir, and S. Sibiryakov, “Ultralight Dark Matter Resonates with Binary Pulsars,” *Phys. Rev. Lett.* **118**, 261102 (2017), [arXiv:1612.06789](#).
  - [14] I. De Martino, T. Broadhurst, S. H. H. Tye, T. Chiueh, H.-Y. Schive, and R. Lazkoz, “Recognising Axionic Dark Matter by Compton and de-Broglie Scale Modulation of Pulsar Timing,” *Phys. Rev. Lett.* **119**, 221103 (2017), [arXiv:1705.04367](#).
  - [15] G.-W. Yuan, Z.-Q. Xia, C. Tang, Y. Zhao, Y.-F. Cai, Y. Chen, J. Shu, and Q. Yuan, “Testing the alp-photon coupling with polarization measurements of sagittarius a\*,” *Journal of Cosmology and Astroparticle Physics* **2021**, 018 (2021).
  - [16] G.-W. Yuan, Z.-Q. Shen, Y.-L. S. Tsai, Q. Yuan, and Y.-Z. Fan, “Constraining ultralight bosonic dark matter with keck observations of s2’s orbit and kinematics,” *Phys. Rev. D* **106**, 103024 (2022).
  - [17] H.-K. Guo, Y. Ma, J. Shu, X. Xue, Q. Yuan, and Y. Zhao, “Detecting dark photon dark matter with gaia-like astrometry observations,” *Journal of Cosmology and Astroparticle Physics* **2019**, 015 (2019).
  - [18] K. Nomura, A. Ito, and J. Soda, “Pulsar timing residual induced by ultralight vector dark matter,” *European Physical Journal C* **80**, 419 (2020), [arXiv:1912.10210](#).
  - [19] M. Fabbrichesi, E. Gabrielli, and G. Lanfranchi, “The Dark Photon,” [arXiv e-prints](#), [arXiv:2005.01515](#) (2020), [arXiv:2005.01515](#).
  - [20] A. Caputo, A. J. Millar, C. A. J. O’Hare, and E. Vitagliano, “Dark photon limits: A handbook,” *Phys. Rev. D* **104**, 095029 (2021), [arXiv:2105.04565](#).
  - [21] X. Xue *et al.* (PPTA Collaboration), “High-precision search for



- dark photon dark matter with the Parkes Pulsar Timing Array,” *Phys. Rev. Res.* **4**, L012022 (2022), [arXiv:2112.07687](#).
- [22] J. M. Armaleo, D. López Nacir, and F. R. Urban, “Pulsar timing array constraints on spin-2 ULDM,” *JCAP* **09**, 031 (2020), [arXiv:2005.03731](#).
- [23] S. Sun, X.-Y. Yang, and Y.-L. Zhang, “Pulsar timing residual induced by wideband ultralight dark matter with spin 0,1,2,” *Phys. Rev. D* **106**, 066006 (2022), [arXiv:2112.15593](#).
- [24] G. Hobbs *et al.*, “The International Pulsar Timing Array project: using pulsars as a gravitational wave detector,” *Classical and Quantum Gravity* **27**, 084013 (2010), [arXiv:0911.5206](#).
- [25] G. Hobbs, “Pulsars as gravitational wave detectors,” in *High-Energy Emission from Pulsars and their Systems*, Astrophysics and Space Science Proceedings, Vol. 21 (2011) p. 229, [arXiv:1006.3969](#).
- [26] A. Khmelnitsky and V. Rubakov, “Pulsar timing signal from ultralight scalar dark matter,” *JCAP* **02**, 019 (2014), [arXiv:1309.5888](#).
- [27] N. K. Porayko *et al.*, “Parkes Pulsar Timing Array constraints on ultralight scalar-field dark matter,” *Phys. Rev. D* **98**, 102002 (2018), [arXiv:1810.03227](#).
- [28] X. Xue *et al.*, “Constraining Cosmological Phase Transitions with the Parkes Pulsar Timing Array,” *Phys. Rev. Lett.* **127**, 251303 (2021), [arXiv:2110.03096](#).
- [29] D. E. Kaplan, A. Mitridate, and T. Trickle, “Constraining fundamental constant variations from ultralight dark matter with pulsar timing arrays,” *Phys. Rev. D* **106**, 035032 (2022), [arXiv:2205.06817](#).
- [30] Y.-M. Wu *et al.*, “Constraining ultralight vector dark matter with the Parkes Pulsar Timing Array second data release,” *Phys. Rev. D* **106**, L081101 (2022), [arXiv:2210.03880](#).
- [31] R. N. Manchester *et al.*, “The Parkes Pulsar Timing Array Project,” *Publ. Astron. Soc. Australia* **30**, e017 (2013), [arXiv:1210.6130](#).
- [32] M. Kerr *et al.*, “The Parkes Pulsar Timing Array project: second data release,” *Publ. Astron. Soc. Australia* **37**, e020 (2020), [arXiv:2003.09780](#).
- [33] M. Kramer and D. J. Champion, “The european pulsar timing array and the large european array for pulsars,” *Classical and Quantum Gravity* **30**, 224009 (2013).
- [34] G. Desvignes *et al.*, “High-precision timing of 42 millisecond pulsars with the European Pulsar Timing Array,” *Mon. Not. R. Astron. Soc.* **458**, 3341 (2016), [arXiv:1602.08511](#).
- [35] M. A. McLaughlin, “The north american nanohertz observatory for gravitational waves,” *Classical and Quantum Gravity* **30**, 224008 (2013).
- [36] Z. Arzoumanian *et al.*, “The nanograv 12.5 yr data set: Search for an isotropic stochastic gravitational-wave background,” *The Astrophysical Journal Letters* **905**, L34 (2020).
- [37] R. Nan, D. Li, C. Jin, Q. Wang, L. Zhu, W. Zhu, H. Zhang, Y. Yue, and L. Qian, “The Five-Hundred Aperture Spherical Radio Telescope (fast) Project,” *International Journal of Modern Physics D* **20**, 989 (2011), [arXiv:1105.3794](#).
- [38] D. Li *et al.*, “FAST in Space: Considerations for a Multibeam, Multipurpose Survey Using China’s 500-m Aperture Spherical Radio Telescope (FAST),” *IEEE Microwave Magazine* **19**, 112 (2018), [arXiv:1802.03709](#).
- [39] M. Ajello *et al.* (Fermi-LAT Collaboration), “A gamma-ray pulsar timing array constrains the nanohertz gravitational wave background,” *Science* **376**, abm3231 (2022), [arXiv:2204.05226](#).
- [40] J. Bovy and S. Tremaine, “On the local dark matter density,” *Astrophys. J.* **756**, 89 (2012), [arXiv:1205.4033](#).
- [41] S. Sivertsson, H. Silverwood, J. I. Read, G. Bertone, and P. Steger, “The local dark matter density from SDSS-SEGUE G-dwarfs,” *Mon. Not. Roy. Astron. Soc.* **478**, 1677 (2018), [arXiv:1708.07836](#).
- [42] C. P. Burgess, J. P. Conlon, L.-Y. Hung, C. H. Kom, A. Maharana, and F. Quevedo, “Continuous Global Symmetries and Hyperweak Interactions in String Compactifications,” *JHEP* **07**, 073 (2008), [arXiv:0805.4037](#).
- [43] M. Goodsell, J. Jaeckel, J. Redondo, and A. Ringwald, “Naturally Light Hidden Photons in LARGE Volume String Compactifications,” *JHEP* **11**, 027 (2009), [arXiv:0909.0515](#).
- [44] M. Cicoli, M. Goodsell, J. Jaeckel, and A. Ringwald, “Testing String Vacua in the Lab: From a Hidden CMB to Dark Forces in Flux Compactifications,” *JHEP* **07**, 114 (2011), [arXiv:1103.3705](#).
- [45] A. Pierce, K. Riles, and Y. Zhao, “Searching for Dark Photon Dark Matter with Gravitational Wave Detectors,” *Phys. Rev. Lett.* **121**, 061102 (2018), [arXiv:1801.10161](#).
- [46] K. Aoki and K.-i. Maeda, “Condensate of Massive Graviton and Dark Matter,” *Phys. Rev. D* **97**, 044002 (2018), [arXiv:1707.05003](#).
- [47] L. Marzola, M. Raidal, and F. R. Urban, “Oscillating Spin-2 Dark Matter,” *Phys. Rev. D* **97**, 024010 (2018), [arXiv:1708.04253](#).
- [48] R. N. Manchester, G. B. Hobbs, A. Teoh, and M. Hobbs, “The Australia Telescope National Facility Pulsar Catalogue,” *Astron. J.* **129**, 1993 (2005), [arXiv:astro-ph/0412641](#).
- [49] Z. Arzoumanian *et al.* (NANOGrav Collaboration), “The NANOGrav 11-year Data Set: Pulsar-timing Constraints On The Stochastic Gravitational-wave Background,” *Astrophys. J.* **859**, 47 (2018), [arXiv:1801.02617](#).
- [50] J. Bergé, P. Brax, G. Métris, M. Pernot-Borràs, P. Touboul, and J.-P. Uzan, “MICROSCOPE Mission: First Constraints on the Violation of the Weak Equivalence Principle by a Light Scalar Dilaton,” *Phys. Rev. Lett.* **120**, 141101 (2018), [arXiv:1712.00483](#).
- [51] J. Luo *et al.*, “PINT: A Modern Software Package for Pulsar Timing,” *Astrophys. J.* **911**, 45 (2021), [arXiv:2012.00074](#).
- [52] J. A. Ellis, M. Vallisneri, S. R. Taylor, and P. T. Baker, “Enterprise: Enhanced numerical toolbox enabling a robust pulsar inference suite,” Zenodo (2020).
- [53] J. Ellis and R. van Haasteren, “jellis18/ptmcmcsmpl: Official release,” (2017).
- [54] S. S. Wilks, “The Large-Sample Distribution of the Likelihood Ratio for Testing Composite Hypotheses,” *The Annals of Mathematical Statistics* **9**, 60 (1938).
- [55] Y. Z. Fan *et al.*, “Very Large Area Gamma-ray Space Telescope (VLAST),” *Acta Astronomica Sinica* **63**, 27 (2022).